# Photoinduced Charge Generation in a Molecular Bulk Heterojunction Material

Loren G. Kaake,*,[†] Jacek J. Jasieniak,[†] Ronald C. Bakus, II,[∥] Gregory C. Welch,[⊥] Daniel Moses,[†] Guillermo C. Bazan,[†,§,∥] and Alan J. Heeger[†,‡,§]

[†]Center for Polymers and Organic Solids, [‡]Department of Physics, [§]Materials Department, and [∥]Chemistry Department, University of California—Santa Barbara, Santa Barbara, California 93106, United States
[⊥]Department of Chemistry, Dalhousie University, Halifax, NS, Canada

ABSTRACT: Understanding the charge generation dynamics in organic photovoltaic bulk heterojunction (BHJ) blends is important for providing the necessary guidelines to improve overall device efficiency. Despite more than 15 years of experimental and theoretical studies, a universal picture describing the generation and recombination processes operating in organic photovoltaic devices is still being forged. We report here the results of ultrafast transient absorption spectroscopy measurements of charge photo-generation and recombination processes in a high-performing solution-processed molecular BHJ. For comparison, we also studied a high-performing polymer-based BHJ material. We find that the majority of charge carriers in both systems are generated on <100 fs time scales and posit that excited state delocalization is responsible for the ultrafast charge transfer. This initial delocalization is consistent with the fundamental uncertainty associated with the photon absorption process (in the visible, $\lambda/4\pi$ > 30 nm) and is comparable with the phase-separated domain size. In addition, exciton diffusion to charge-separating heterojunctions is observed at longer times (1−500 ps). Finally, charge generation in pure films of the solution processed molecule was studied. Polarization anisotropy measurements clearly demonstrate that the optical properties are dominated by molecular (Frenkel) exictons and delocalized charges are promptly produced (t < 100 fs).
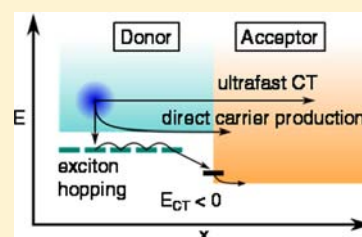
INTRODUCTION

Steady advances in the efficiencies of organic solar cells[1−5] have been accompanied by a more detailed understanding of the mechanism by which mobile charges are generated.[6−8] The active region in a solution-processed organic solar cell is a mixed film of electron-donating and electron-accepting materials known as a bulk heterojunction (BHJ). In earlier work, the electron donor has been a semiconducting polymer, but recent awareness of challenges imposed by purity and batch-to-batch variation has led to the development of solution-processed electron-donating molecules.[9−11] When blended with fullerenes, the most common electron acceptor, these systems show promising performance.[4,12] From a fundamental point of view, the development of any new photovoltaic material begs the question regarding the relevance of pre-existing models in describing the photophysics of charge generation.

The currently accepted model of carrier photogeneration describes the process as beginning with the excitation of a localized and bound electron−hole pair called a Frenkel exciton (an intramolecular excitation). The exciton moves diffusively until it encounters a donor−acceptor interface, where charge transfer is energetically favorable. The result of the charge transfer process has been described as a bound interfacial pair called a charge transfer (CT) exciton, which separates into mobile charge carriers via a mechanism that has yet to be definitively identified.[13−16] In contrast to this exciton diffusion picture, ultrafast generation of mobile carriers (t < 100 fs) is

observed and, in fact, accounts for a large percentage of the total yield.[17]

We address the problem of carrier photogeneration in a solution-processed BHJ comprised of the molecular donor p-DTS(PTTh$_2$)$_2$[12] and the common electron acceptor PC$_{70}$BM (see Figure 1a for molecular structures). We use transient absorption spectroscopy to monitor the dynamics of charge carriers in p-DTS(PTTh$_2$)$_2$ that are generated after the absorption of a 400 nm pulse of light. In order to establish a relationship between the charge generation dynamics of this molecular BHJ with the more well-known polymer systems, we also study the PCDTBT:PC$_{70}$BM BHJ material[18] (molecular structure also shown in Figure 1).

The second part of this work focuses on the yet unreported photodynamics of p-DTS(PTTh$_2$)$_2$ in order to clarify several questions that are important to understanding the charge generation mechanism of a BHJ solar cell. Of particular importance is the nature of the primary photoexcitations and their relationship to mobile carriers. A model for charge separation uses the language and concepts derived from an understanding of these elementary processes, and subtle clarifications of these issues can do much to alleviate points of confusion.

The problem of understanding the relationship between elementary photoexcitations and charge carriers can be

p-DTS(PTTh₂)₂

5,5'-bis{(4-(7-hexylthiophen-2-yl)thiophen-2-yl)-[1,2,5]thiadiazolo
[3,4-c]pyridine-3,3'-di-2-ethylhexylsilylene-2,2'-bithiophene

PCDTBT

poly[N-9"-heptadecanyl-2,7
carbazole-alt-5,5-(4',7'-di2-thienyl-
2',1',3'-benzothiadiazole

PC₇₀BM
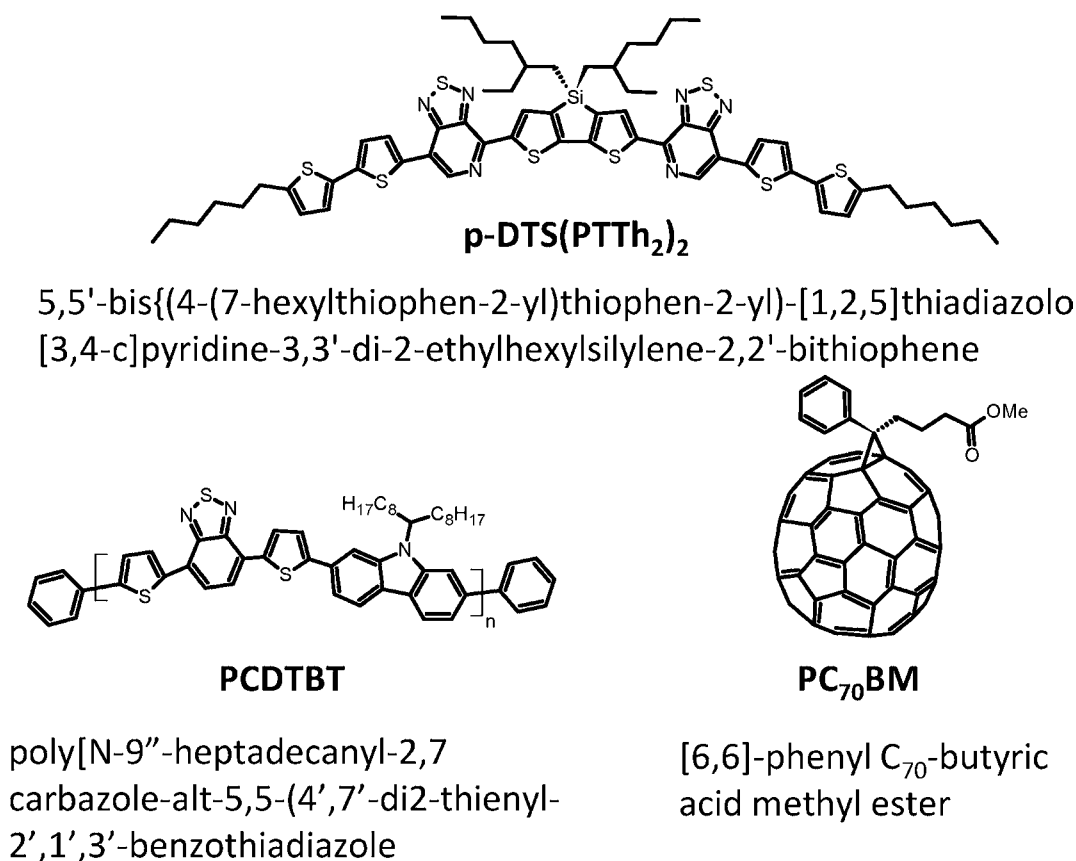
[6,6]-phenyl C_{70}-butyric
acid methyl ester

Figure 1. Compounds used in this study.

approached by investigating the photoconductive response of the pure material. The commonly held viewpoint is that photoexciting an organic solid results in highly localized and strongly bound Frenkel excitons. The dissociation of Frenkel excitons is typically discussed in terms of the Onsager–Braun model, originally devised to describe photoionization of gaseous molecules[19] and later extended to describe exciton dissociation in the presence of an electric field.[20] In this model, electrons and holes are thought to be highly localized ($r = \sim 1$ nm), allowing one to neglect electronic interactions between neighboring molecules. The high degree of localization implies that the Coulomb binding energy between electrons and holes contributes significantly to stabilize bound excitons relative to separated and uncorrelated electron–hole pairs. This energy, called the exciton binding energy, is estimated to be between 1 and 0.1 eV. In the large binding energy limit, one could rightly call the material an insulator, as it would possess negligible photoconductive response within the UV–visible–IR regions of the spectrum. In the case where the photon energy was sufficiently large to overcome the exciton binding energy, carriers could be produced efficiently. Therefore, one of the main indicators for strong exciton binding energies is a photoconductive response that changes as a function of wavelength, conspicuously increasing at some threshold photon energy.

The existence of strongly bound Frenkel excitons creates a challenge of understanding charge separation in any context, even in the case of bulk heterojunctions, where a type 2 interface provides the driving force for charge separation. The results of the first two sections are discussed in terms of the general problem of charge photogeneration in organic photo-

voltaic systems. Particular attention is paid to the separation of CT excitons, a problem of widespread interest. In addition, the importance of ultrafast carrier generation processes is high-lighted.

■ **EXPERIMENTAL SECTION**

Films used in transient absorption and fluorescence experiments were spin-cast onto 0.5 in. sapphire disks that were cleaned with piranha solutions for at least 24 h. Sapphire disks were rinsed with deionized water and 2-propanol prior to drying with a dry nitrogen stream. Photoconductivity and absorptance measurements were conducted on glass substrates. All films were spin-cast and annealed inside of a glovebox. Samples were held under high vacuum ($p \approx 10^{-6}$ Torr) during the transient absorption and photoconductivity measurements.

Pure films of p-DTS(PTTh₂)₂ were spin-cast from chlorobenzene solutions at a concentration of 40 mg/mL using a spin speed of 1500 rpm. Films were annealed at 60 °C to drive out residual solvent. Bulk heterojunction films of p-DTS(PTTh₂)₂:PC₇₀BM (7:3 w/w) were prepared in a manner analogous to those used in device fabrication.[21] Films were spin-cast from chlorobenzene solutions (40 mg/mL) that contained a small amount of solvent additive (0.25% 1,8-diiodooctane v/v). Films were cast at 1700 rpm and annealed for 10 min at 70 °C. Bulk heterojunction films of PCDTBT:PC₇₀BM (1:4 w/w) were prepared as described in detail in previous reports[18] from a solution of 1,2-dichlorobenzene/chlorobenzene (3:1 v/v). Films were spin-cast at 4000 rpm and annealed at 60 °C to drive out residual solvent.

Absorptance was determined from the measured transmittance and reflectance of thin films deposited on low-sodium glass substrates using a Perkin-Elmer Lambda 780 NIR–UV–vis spectrometer coupled to an integrating sphere attachment. Photoconductivity measurements were performed in a lateral direction on thin-film samples with gold electrodes using a Keithley 487 picoammeter in conjunction with a Stanford Instruments SR830 lock-in amplifier. A mechanically chopped, monochromated tungsten lamp served as the
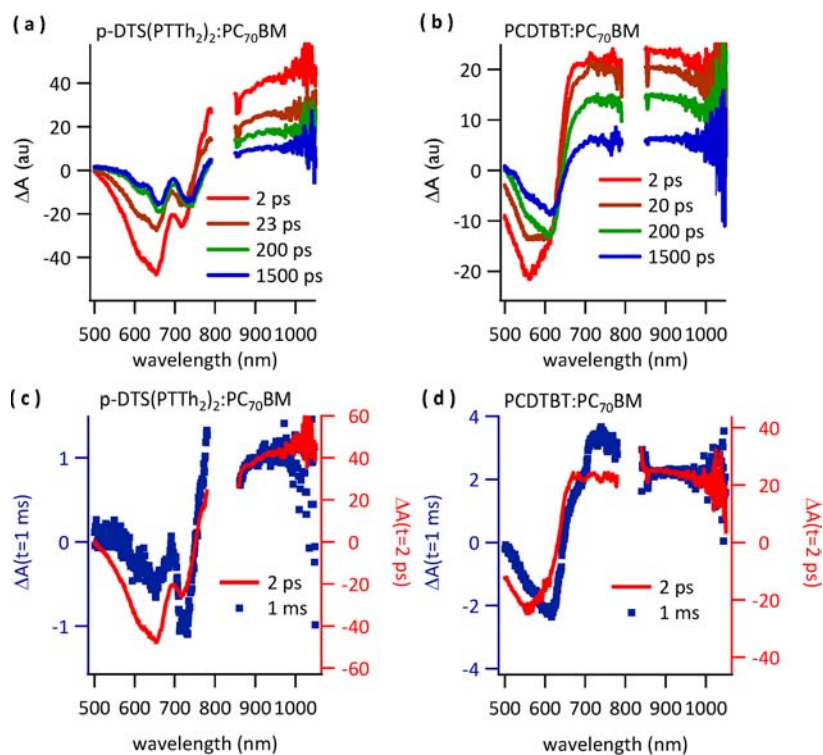
Figure 2. Transient absorption spectra. (a) Spectra collected from a p-DTS(PTTh$_2$)$_2$:PC$_{70}$BM BHJ material. Pump intensity was 100 μJ cm^{-2}. (b) Spectra collected from a PCDTBT:PC$_{70}$BM BHJ material. Pump intensity was 200 μJ cm^{-2}. (c) Spectra collected from a p-DTS(PTTh$_2$)$_2$:PC$_{70}$BM BHJ material at 2 ps (red lines, right axis) and 1 ms (blue dots, left axis); range of axes was adjusted such that they share the same zero and the signal intensities matched in the near-IR. Part d is the same as part c but with a PCDTBT:PC$_{70}$BM BHJ material.

excitation source in the photoconductivity experiment. Photocurrent was referenced to a calibrated silicon photodiode.

Fluorescence measurements were conducted using a custom-built fluorimeter. Excitation was accomplished with the 457 nm line of an Ar$^+$ laser (Spectraphysics Beamlok 2065). The fluorescence was collected by a system of lenses and dispersed by a Cherny−Turner monochromator (Acton SP-500). The spectra were recorded using a spectroscopic CCD camera with a Si sensor (Princeton Instruments PIXIS:400). The emission spectra were corrected for the instrument's spectral response inhomogeneity by taking a spectrum of a calibrated tungsten lamp (Ocean Optics LS-1) and determining the necessary correction factors.

Transient absorption measurements were conducted with a pulsed laser system at a repetition rate of 1 kHz. The laser consists of a titanium sapphire oscillator (Spectra Physics Tsunami) that is pumped with a Nd:VO$_4$ laser (Spectra Physics Millenia). The pulses are fed into a regenerative amplifier (Spectra Physics Spitfire) that is pumped with a high-power Nd:YLF laser (Spectra Physics Empower); 790 nm pulses were generated with a pulse width of 100 fs. The pulses were split into pump and probe paths. The pump pulse was frequency-doubled to 395 nm and focused onto the sample with a beam diameter of 1 mm and pulse energies of 0.3−120 μJ/cm^2. The pump pulse was put through a delay stage to achieve time resolution. The probe pulse was focused into a 1 mm sapphire disk in order to generate the white light continuum used to measure visible and near-IR spectra. The probe pulse was split before reaching the sample to provide a reference path to aid in the correction of intensity fluctuations. The subtraction was aided by careful collimation of the white light probe. In addition, synchronous chopping of the probe enabled the subtraction of an accurate dark count reading, which tends to drift over time. All spectra were manually corrected for the temporal chirp present in the white light continuum. The polarization angle between pump and probe beams was 54° ± 1° unless otherwise noted. Lastly, spectra were collected with a silicon CCD camera that was calibrated using a series of narrow band-pass filters.

RESULTS

Spectral Features of p-DTS(PTTh$_2$)$_2$:PC$_{70}$BM and PCDTBT:PC$_{70}$BM BHJ Materials. In order to monitor charge photogeneration and recombination dynamics, the spectral signature of charge carriers must first be unambiguously identified. To do this, we compared transient absorption spectra of both p-DTS(PTTh$_2$)$_2$:PC$_{70}$BM and PCDTBT:PC$_{70}$BM BHJ's at 2 ps and 1 ms (Figure 2c,d). The spectral match in the region 500−800 nm is poor; however the agreement in the near-IR (850−1000 nm) is significantly better. The 1 ms spectra are free of excitons and are dominated by the charge carriers, which would contribute to photocurrent in a solar cell or photoconductor. Thus, the near-IR photoinduced absorption is that of charge carriers. Because the 2 ps spectra have nearly identical line shapes in the near-IR (850−1000 nm) as the 1 ms spectra, and the near-IR line shape is not time-dependent (see Figure 2a,b), the near IR photoinduced absorption can be integrated to provide a probe of the charge carrier population. This assignment agrees with previous reports on a molecule of similar structure to p-DTS(PTTh$_2$)$_2$,[22] and previous reports on PCDTBT.[17,23] The photobleaching signal exhibits a red-shift as a function of time, possibly arising from energy migration,[17] although thermal effects[24] and acoustic phonons[22] might also contribute.

Dynamics of p-DTS(PTTh$_2$)$_2$:PC$_{70}$BM and PCDTBT:PC$_{70}$BM BHJ Materials. The extracted population dynamics of photoinduced holes was measured at different pump fluences and is shown in Figure 3. Each trace was normalized to its value at 100 fs and its value at negative time scales was set to zero (in effect, subtracting the 1 ms signal). The short time scale behavior found in Figure 3a indicates that a large component of the charge transfer in p-DTS-
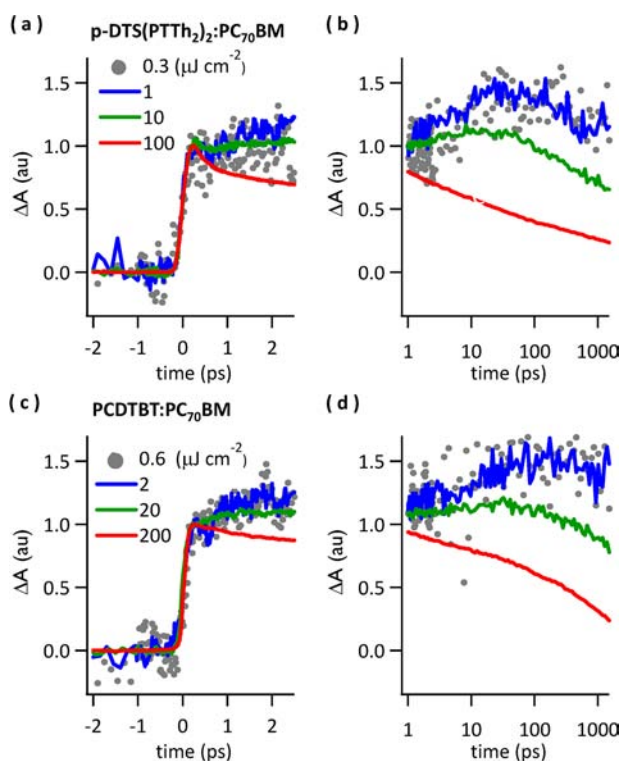
Figure 3. Near infrared dynamics. (a) Short time scale traces of p-DTS(PTTh$_2$)$_2$:PC$_{70}$BM blends. (b) Long time scale traces from the same experiment as in part a. (c) Short time scale traces of PCDTBT:PC$_{70}$BM blends. (d) Long time scale traces from the same experiment as in part c. The dynamics was extracted by integrating the near-IR photoinduced absorption over 850−1000 nm. Extracted dynamics was insensitive to the limits of integration within this range.

(PTTh$_2$)$_2$:PC$_{70}$BM is ultrafast. As shown above, the near-IR signature of the charge carrier population was identified with the formation of self-localized polarons in semiconducting polymers. The formation of the distortions that define the polaron have been time-resolved.[25] In agreement with the theoretical predictions by Su and Schrieffer,[26] polaron formation occurs within approximately 10^{-13} s, i.e., roughly within the period of an intrachain optical phonon. Thus, the ultrafast component of the charge transfer occurs prior to the self-localization associated with polaron formation.

The magnitude of the short time scale signal is linear over the 2 orders of magnitude in the pump intensity used in both systems. In contrast, the long time scale charge transfer component found in Figure 3b rises after approximately 20−50 ps and appears only at pump powers sufficiently low that bimolecular decay (exciton-charge and exciton−exciton annihilation) becomes negligible.[27−29] In the case of PCDTBT:PC$_{70}$BM (Figure 3d) the slower charge transfer component rises until 100−500 ps. Importantly, even the slower charge transfer component dynamics is pump-power-independent at the lowest pump fluences studied.

To estimate the instantaneous excitation density at the lowest pump power (0.3 μJ/cm^2), one can assume that every photon is absorbed. Given a film thickness of ~100 nm, the lowest excitation density studied in p-DTS(PTTh$_2$)$_2$:PC$_{70}$BM was ~6×10^{16} cm^{-3}, which is comparable to the mobile carrier density in a working solar cell under illumination by the radiation from 1 sun. In PCDTBT:PC$_{70}$BM (Figure 3c,d), the lowest excitation density studied was ~1×10^{17}. To restate, in

both materials there are two easily distinguishable components to the photoinduced charge generation, an ultrafast component, the intensity of which is linear in pump power, and a slower rising component, which is observed at lower pump fluence.

Two Pathways for Exciton Splitting in p-DTS-(PTTh$_2$)$_2$:PC$_{70}$BM and PCDTBT:PC$_{70}$BM BHJ Materials. The different power dependence displayed by the ultrafast charge generation process compared to the slowly rising component clearly indicates that two qualitatively different mechanisms are operating. The slow-rising component, which is strongly affected by the pump intensity, is due to exciton diffusion. As stated previously, high excitation densities can give rise to nonlinear recombination processes, such as exciton−exciton annihilation and charge−exciton recombination.[27−29] These processes quench diffusing excitons before they can reach a charge-separating heterojunction interface. Thus, exciton diffusion dynamics will only be observed at low excitation densities, as is the case reported here.

It is not immediately obvious, however, whether the excitons are diffusing from fullerene domains or from domains of the electron donor. Because the 400 nm pump pulse excites the fullerene as well as the electron donor, it is reasonable to assume that some part of the diffusive component arises from the fullerene. To address this question, we first observe that the dynamics of exciton diffusion is faster in p-DTS-(PTTh$_2$)$_2$:PC$_{70}$BM than in PCDTBT:PC$_{70}$BM. This immediately implies that exciton diffusion within the donor plays an important role in the observed dynamics. This observation is confirmed by looking at the dynamics of the photobleach signal. If holes are being transferred into the donor from the fullerene, the photobleach will increase in intensity with time. Conversely, if hole transfer does not occur, and most charges are the result of electron transfer to the fullerene, the intensity of the bleaching signal should be conserved; the strength of the photobleach should not be sensitive to whether it is being caused by an exciton or a hole. In the case of p-DTS(PTTh$_2$)$_2$:PC$_{70}$BM, no such increase is seen. However, some increase (approximately 30%) in the photobleach is observed in PCDTBT:PC$_{70}$BM heterojunctions, indicating a significant amount of hole transfer to the donor following exciton diffusion in the fullerene. This observation is consistent with the amount of fullerene in each sample. PCDTBT:PC$_{70}$BM heterojunctions are comprised of 80% fullerene, while p-DTS(PTTh$_2$)$_2$:PC$_{70}$BM heterojunctions contain 30% fullerene by weight. In summary, the slower rise times of the mobile carrier signal are related to exciton dynamics in both components, but the observed dynamics in p-DTS(PTTh$_2$)$_2$:PC$_{70}$BM BHJ's is primarily from excitons in p-DTS(PTTh$_2$)$_2$.

The short time scale (<100 fs) dynamics shows qualitatively different power dependence than the longer time scale exciton diffusion dynamics. The electron transfer between polymer and fullerenes is known to be <100 fs.[30,31] Because any acceptor molecule *directly* in contact with a fullerene should display this behavior, it has been proposed that all short time scale charge generation phenomena are a result of this process. We believe this interpretation is oversimplified and incorrect. Barring incredible coincidence, this is inconsistent with the data; PCDTBT:PC$_{70}$BM contains 80% fullerene while p-DTS-(PTTh$_2$)$_2$:PC$_{70}$BM contain only 30% by weight, yet in both samples, the charge carrier absorption signal rises to 70% of its maximum intensity within less than 100 fs. Moreover, the dominant contribution of the ultrafast charge transfer in

comparison with diffusive charge transfer is observed in other systems.[32−34] That the degree of intermixing should be so high and so similar from sample to sample is itself a bold claim, despite the fact that fullerene derivatives are known to possess a degree of miscibility in a variety of donor materials.[35−39] More specifically, similar behavior is observed in poly(3-hexylthiophene) (P3HT) heterojunctions, where the fullerene miscibility is limited to amorphous regions of material.[38] Regiorandom P3HT is almost totally amorphous, and BHJ materials made from it show strong geminate recombination, as shown by Guo et al.[33] However, in regioregular P3HT the ultrafast charge transfer component is highly efficient at producing mobile charges.[33] In other words, the assumption that all short time scale charge generation is wholly due to intimate contact between the donor and fullerene is not consistent with the data, because ultrafast carrier generation does not suffer the geminate recombination losses expected from regions of low phase purity.[40] The same recombination argument is valid for the intercalated structure investigated by the McGehee group.[35,37] Concentrations of fullerene must be high enough to create phase-separated structures in order to achieve moderate solar cell efficiencies. A definitive test for geminate recombination was published by Street and co-workers, which unambiguously demonstrated the absence of significant geminate recombination in PCDTBT and P3HT. This test should be applied to any system where geminate recombination is thought to play a role. We also note that the PCDTBT BHJ system has an internal quantum efficiency approaching 100%, implying that essentially every absorbed photon results in a separated pair of charge carriers and that all carriers are collected at the electrodes, leaving little room for significant geminate recombination.[18]

Ultrafast Charge Transfer: The Role of Fundamental Uncertainty. Alternative hypotheses of the ultrafast charge carrier process require that the nature of the initial photo-excitation is not the trivial photoexcitation of a single molecule or chromophoric unit. The fission of singlet excitons into two triplets[41−45] and relatively long-lived coherence[46,47] imply that there is complexity in the initial photoexcited state. Understanding that complexity is critical to understanding the ultrafast charge separation process.

Consider the fundamental uncertainty associated with the absorption of a 3 eV photon. Time−energy uncertainty dictates that one cannot know when the energy leaves the photon field with a precision better than 0.5 fs. More interestingly, the position−momentum uncertainty relationship, $\Delta x \Delta p \geq \hbar/2$, dictates that one cannot know the location of the excitation created by the absorption to an accuracy greater than about $\lambda/4\pi > 30$ nm. In other words, the initial photoexcitation is delocalized but must undergo rapid localization, or wave function collapse, on the order of the decoherence time scale (∼25 fs in a phenylene vinylene derivative, MEH-PPV).[46] By assuming that photoexcitation results only in highly localized Frenkel excitons, one implicitly assumes that the wave function localization process is trivial. One way to evaluate this hypothesis in these systems is to examine the products of the initial photoexcitation process, looking for products in addition to intramolecular excitations that are generated on ultrafast time scales. In addition, Figure 4 shows evidence of coherent effects in the p-DTS(PTTh$_2$)$_2$ BHJ. At early time scales, the absorption line shape possesses a sinusoidal variation around 700 nm, indicating an interaction between the electromagnetic field of the probe pulse with a coherent excited state
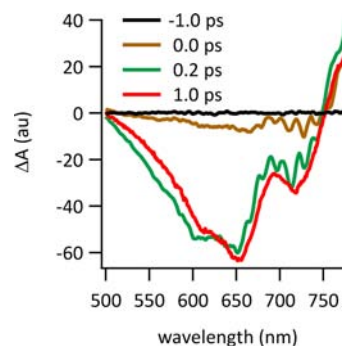
Figure 4. Transient absorption spectra of p-DTS(PTTh$_2$)$_2$:PC$_{70}$BM films at short time scales.

population.[48] As expected of a coherent effect, the sinusoidal features vanish by 1 ps.

Charge Photogeneration in Pure Films of p-DTS-(PTTh$_2$)$_2$. As alluded to above, excited state delocalization on the basis of the uncertainty principle is one way in which charge ultrafast charge transfer could occur over length scales in the 10−20 nm range. Experiments on pure films of p-DTS-(PTTh$_2$)$_2$ must show evidence that such effects should they play an important role in the photophysics of the material. We compare the photoconductivity and absorptance of p-DTS-(PTTh$_2$)$_2$ thin films in Figure 5. The absorptance spectrum
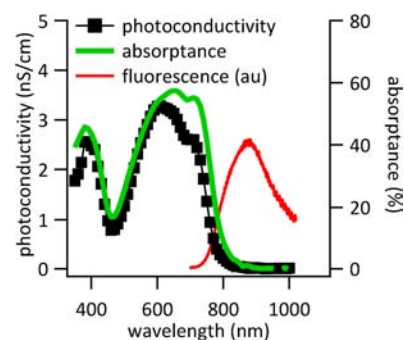

Figure 5. Basic observations in pure p-DTS(PTTh$_2$)$_2$ films. Photoconductive response (squares), absorptance (thick green line), and fluorescence (thin red line) of the molecular film.

shows the vibronic splitting typical of excitonic transitions in the solid state. In addition, the fluorescence spectrum is displayed. As expected, the fluorescence spectrum exhibits a significant Stokes shift, but its vibronic progression is obscured, presumably by energetic disorder. More surprisingly, the photoconductive response tracks the absorptance relatively accurately across the entire spectrum, despite the fact that the initial absortion is that of an intramolecular Frenkel exciton. This is in stark contrast with what is observed in the fullerenes, where the photoconductive response increases sharply upon reaching an energy ∼0.4 eV above the optical gap.[49] By the mere fact that photoconductivity probes the relative spectral probability of charge carrier formation and collection, this result suggests that even the lowest energy transitions in p-DTS(PTTh$_2$)$_2$ are capable of generating long-lived mobile carriers.

Spectral Assignments in Pure Films of p-DTS(PTTh$_2$)$_2$. In traditional molecular crystals, the formation of free charge carriers via intramolecular transitions is known to be obstructed by high exciton binding energies. The above findings suggest

that this simple picture of the formation of such carriers cannot be complete. To gain deeper insight into the charge generation mechanism, we employed transient absorption spectroscopy. In Figure 6, we show transient spectra of photoexcited *p*-
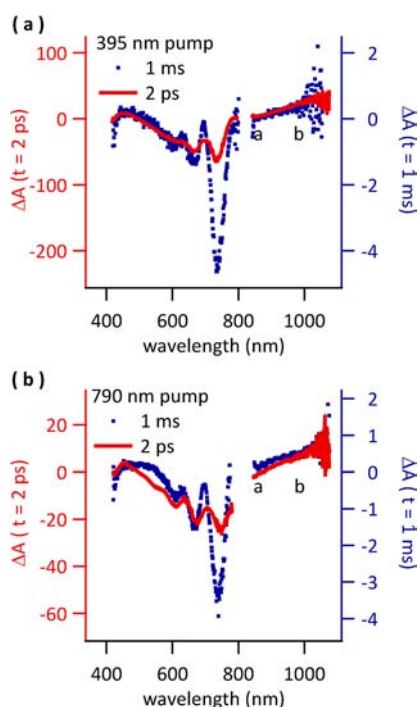

Figure 6. Transient absorption spectra of pure *p*-DTS(PTTh$_2$)$_2$. (a) Spectra taken at 1 ms (blue dots) and 2 ps (red line) after a pump pulse of 395 nm. (b) Spectra taken at 1 ms (blue dots) and 2 ps (red line) after a pump pulse of 790 nm.

DTS(PTTh$_2$)$_2$ at excitation wavelengths of 790 or 395 nm. Similar to the above results on *p*-DTS(PTTh$_2$)$_2$:PC$_{70}$BM heterojunctions, we observe a carrier population at a time delay of 1 ms that is large enough to detect. This signature is characterized by a negative-pointing photobleach in the visible wavelength range and a positive-pointing photoinduced absorption in the near-infrared. At much shorter time scales, the number of charge carriers is much higher, and a population of intramolecular excitations should be expected, consistent with the finite fluorescence yield. By examining the near-infrared region of Figure 6a, one obtains good spectral agreement between the 1 ms spectra and the 2 ps spectra, indicating that charge carriers are present at the shortest time scales.

In the near IR spectral region, fluorescence from photoexcited *p*-DTS(PTTh$_2$)$_2$ would contribute to stimulated emission, resulting in a negative absorbance signature (see Figure 5). This is reflected by a lack of agreement between 2 ps and 1 ms spectra in the wavelength region "a" in Figure 6b. As stated above, this is due to the stimulated emission associated with the fluorescence band of *p*-DTS(PTTh$_2$)$_2$, as can be observed by comparing region a in the transient absorption spectra with the fluorescence spectrum in Figure 5. This band is more obvious when the film is pumped with 790 nm light (Figure 6b) instead of 395 nm light (Figure 6a) because fewer carriers are initially generated at the longer wavelengths. In addition, this band is not observed in the transient absorption of blended films, where the near-infrared signal is insensitive to wavelength, presumably because of photoluminescence quenching.

The most striking difference between the 2 ps and 1 ms spectra is the shape of the photobleaching signal (500−750 nm). More specifically, the relative strength of the peaks that
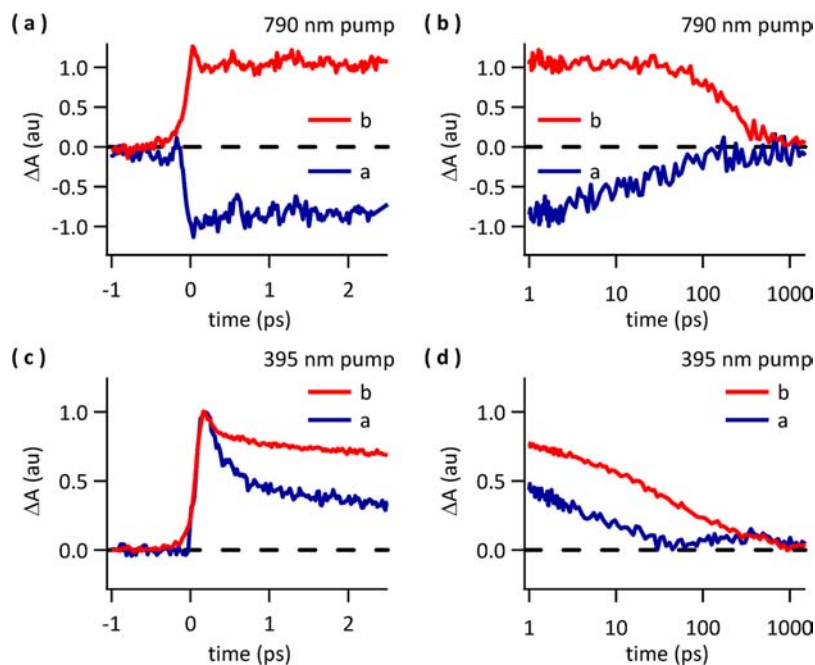
Figure 7. Transient absorption dynamics in the near-infrared for pure *p*-DTS(PTTh$_2$)$_2$. (a) Short time scale dynamics collected with an excitation wavelength of 790 nm for region a (negative-going blue line) and region b (positive-going red line). (b) Long time scale dynamics for the identical data set as the previous panel. (c) Short time scale dynamics collected with an excitation wavelength of 395 nm for region a (blue line) and region b (red line). (d) Long time scale dynamics for the identical data set as the previous panel. (e) Short time scale stimulated emission signal for 790 nm excitation (red line) and 395 nm excitation (blue line). (f) Long time scale dynamics for the identical data set as the previous panel.

make up the photobleach spectrum are very different, in particular the largest peak at 730 nm. One should expect that a significant number of the carriers present at 1 ms are located in energetic traps. Thus, the 1 ms photobleach is determined by the absorption spectrum of the neutral molecules associated with the trapped polarons. Because the position of the photobleaching peaks is similar to those in the absorptance spectrum in Figure 5, the traps are chemically similar or identical to the rest of the film. In addition, the absence of inhomogeneous broadening and the strength of the 0−0 peak in the vibronic progression of the traps imply that the traps are in regions of high crystallinity.[50] This conclusion is in contrast with most assumptions regarding the chemical identity of traps, which correlate them with regions of structural disorder and strong localization. Most of the carriers observed spectroscopically are trapped and do not contribute to the photoconductive response. Trapped polarons have been known and studied for nearly 30 years by modulation spectroscopy. There is a rich literature reporting such data in many systems.[51] Thus, there is no surprise as to the existence of such trapped polarons.

Dynamics in Pure Films of *p*-DTS(PTTh₂)₂. Figure 7 shows the time-dependent transient absorption data obtained from integrating the narrow spectral regions (∼25 nm) labeled "a" and "b" in Figure 6. As described above, region a contains information regarding the kinetics of stimulated emission from singlet excitons in the film, while region b provides a measure of the density of charge carriers. Figure 7a shows the short time scale dynamics of both regions when the film is pumped with 790 nm light; both charge carriers and singlet excitons are instantaneously generated. In Figure 7b one sees the long time scale behavior; the exciton population decays on a time scale expected for photoluminescence decay. In addition, the carrier population does not increase after the initial ultrafast generation and decays on a time scale of 300 ps. Transient photo-conductivity experiments are planned to observe the decay time scale of carriers, which contribute to the photoconductive response in Figure 5.

The absence of any increase in the carrier population after the initial photoexcitation does not correspond to the predictions of the Onsager−Braun model, which describes the carrier generation as requiring energetic activation, and looks different than what is observed in rubrene (especially at the absorption edge).[52] Also no evidence of charge separation following exciton diffusion is observed, a finding in contrast to BHJ films comprised of fullerene and *p*-DTS(PTTh₂)₂, as seen in Figure 3. This indicates that the kinetics do not follow a disorder-induced dissociation model, in contrast with other reports.[53] Finally, the relative amount of carriers generated was linear over a wide range of pump powers (1−150 μJ cm⁻²), and the kinetics was independent of pump power at the lowest powers studied (1−14 μJ cm⁻²). These observations rule out the importance of higher-order processes in the carrier generation dynamics.

The kinetics of carrier photogeneration at shorter pump wavelengths (Figure 7c,d) also indicates that ultrafast carrier generation is the dominant carrier generation pathway; a slow buildup of carriers due to exciton diffusion is not observed. This could be interpreted to indicate a direct coupling between excitons and charge transfer states as proposed by Yamagata et al.[54]

Delocalized Carriers Are Observed via Polarization Anisotropy. Although the primary photoexcitations are intramolecular excitations (Frenkel excitons), mobile charge

carriers are immediately generated (see Figure 7). Determining the identity of the mobile carriers is critical to a meaningful discussion of the carrier photogeneration process. It is unclear, however, from the data presented whether the charge carriers are localized, as in molecular cations and anions, or are more delocalized, as in Bloch waves or mobile polarons.

In order to address this question, we measured the polarization anisotropy of the charge carrier signal (region b). Stated briefly, polarization anisotropy (r) measures the angle between the transition dipole moment of the initial photo-excited state and the one probed at some time delay. This is accomplished by holding the polarization of the probe pulse fixed and varying the polarization of the pump pulse with a half-wave plate, treating the data using the following formula: $r = (I_{\parallel} - I_{\perp})/(I_{\parallel} + 2I_{\perp})$.[55] The experiment was also performed by rotating the probe pulse while the polarization of the pump pulse was left fixed. The results agreed to within the error of the measurement. Polarization anisotropy is a useful measurement in this context because the absorption dipole moment will be different if delocalized carriers are photogenerated or if localized carriers are created. Delocalized carriers will have a transition dipole moment in a direction away from the face of the molecule, where the intermolecular interactions are the strongest, while localized carriers (a molecular anion or cation with wave function confined to a single molecule) will have a transition dipole moment in the plane of the molecule.

In order to quantitatively predict the direction of the absorption dipole moments of the single molecule transitions, we performed density functional theory (DFT) calculations on single gas phase molecules of *p*-DTS(PTTh₂)₂, paying attention to electronic transitions near $\lambda = 395$ and 790 nm. Figure 8b shows that the absorption dipole moment for the lower energy transition is perpendicular to the molecular symmetry axis
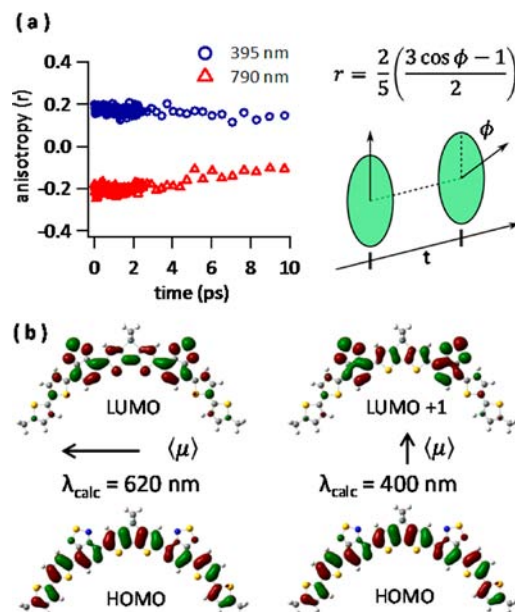
Figure 8. Polarization anisotropy of carrier photogeneration. (a) Polarization anisotropy dynamics taken from region b for excitation wavelengths of 790 nm (red squares) and 395 nm (blue circles). The cartoon describes polarization anisotropy in terms of a time-dependent rotation of a transition dipole moment. (b) DFT calculations showing the major contributions to the electronic transitions probed. The direction of the electronic transition dipole moments μ is also shown.

(parallel to the long axis) while the higher energy transition has an absorption dipole moment parallel to the axis of symmetry (perpendicular to the long axis), as one might naïvely predict. To compare this to the anisotropy measurement, we use the following formula:[55]

$$r = \frac{2}{5}\left(\frac{3\cos[\phi] - 1}{2}\right)$$ (1)

Figure 8a displays the result of a polarization anisotropy experiment for region "b" for pump wavelengths of 395 and 790 nm. The experimentally measured values at vanishing time scales are $r(790 \text{ nm}) = -0.20 \pm 0.1$ and $r(395 \text{ nm}) = 0.18 \pm 0.1$. Using eq 1 we calculate that the absorption dipole moment of the carriers is oriented from the molecular absorption dipole moment at the following angles: $\phi(790 \text{ nm}) = 90°$ and $\phi(395 \text{ nm}) = 51°$. Because the absorption dipole moments at 790 and 395 nm are perpendicular to one another in the plane of the molecule, the absorption dipole moment of the carriers is oriented away from the plane of the molecule. Such a conclusion is only possible when electronic overlap between neighboring molecules cannot be neglected, and the carrier wave functions are delocalized over at least several molecules. Although one-electron bands may exist, the red-shifted absorption of the carriers suggest that they localize to some degree, possibly via intermolecular phonon interactions and/or Coulomb attraction in a manner analogous to polymers.[51] However, the carrier wave function must encompass at least several molecules along the $\pi-\pi$ stacking direction in order to explain the observed polarization anisotropy. To restate, localized electronic transitions (Frenkel excitons) are observed to immediately produce carriers in p-DTS(PTTh$_2$)$_2$ with significant intermolecular delocalization.

■ DISCUSSION OF THE CHARGE TRANSFER MECHANISMS

In the first part of the paper, we examined the photodynamics of two BHJ films. We observed ultrafast carrier generation and a component related to the diffusion of excitons to the internal heterojunction interfaces. In examining pure films of p-DTS(PTTh$_2$)$_2$, we observed that both intramolecular excitations and mobile carriers are produced on ultrafast time scales. We take this to indicate that the initial photoexcited state is not trivially the population of a highly localized Frenkel exciton but rather a coherent superposition of intramolecular excitations as required by the uncertainty relationship. This coherent state (intramolecular excitations plus delocalized carriers) can yield ultrafast electron transfer to a nearby fullerene domain and, after decoherence, produce localized excitons that diffuse incoherently toward a donor/acceptor interface. In the pure material, electron and hole polarons are produced directly.

The influence of direct carrier production in the donor component of the BHJ material comprising p-DTS(PTTh$_2$)$_2$ is shown in Figure 9, where carrier recombination dynamics of BHJ films and neat films is directly compared. Dynamics in the pure film indicates ultrafast carrier generation. Many of the carriers decay via a first-order process ($\tau_R = 300$ ps). In the blended films, ultrafast carrier generation is also observed, but it is followed by a slower charge generation component ($\tau_{ED} = 4$ ps). The slower process is assigned to the diffusive transport of excitons toward the heterojunction interface. In addition, first-order recombination is observed at longer time scales with a time scale *identical* to that observed in the neat films ($\tau_R = 300$
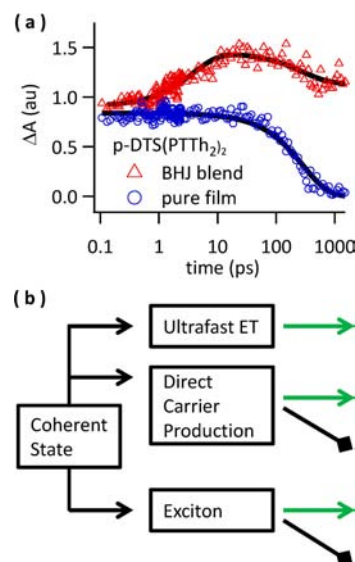
Figure 9. Comparing dynamics of blended and pure films of p-DTS(PTTh$_2$)$_2$. (a) Transient absorption dynamics of carrier absorption. Dynamics of blended film reproduced from Figure 3b. Dynamics of pure film reproduced from Figure 7b. (b) Proposed mechanism of charge photogeneration in p-DTS(PTTh$_2$)$_2$. Green arrows indicate pathways of long-lived carrier generation, and black diamonds indicate recombination mechanisms.

ps). We therefore assign these dynamics to the same mechanism, the recombination of directly (i.e., intrinsic) produced carriers. Importantly, we note that a significant number of the carriers generated on ultrafast time scales ($\sim$65%) do not undergo recombination on the time scales measured here. It is likely that some of the directly produced electrons in p-DTS(PTTh$_2$)$_2$ reach the nearest interface with a fullerene domain and are thus stabilized. The amount of carriers produced through this mechanism versus those produced by the ultrafast electron transfer process is not clear.

Carrier generation processes in p-DTS(PTTh$_2$)$_2$ BHJ films are summarized in Figure 9. Photons are absorbed, creating a coherent state as required by the uncertainty principle (intramolecular excitations plus delocalized carriers) that can yield ultrafast electron transfer to a nearby fullerene domain and, after decoherence, produce localized excitons that diffuse incoherently toward a donor/acceptor interface. In the pure material, electron and hole polarons are produced directly, some of which are stabilized by electron transfer to the fullerene. As stated previously, 70% of all carriers are produced on ultrafast time scales. Of this population, two-thirds are charge separated by the heterojunction interface, while the other one-third recombine on a time scale of 300 ps. As an aside, we note that the efficiency of separating the directly produced carriers may be driven by an internal electric field resulting from the initial difference in Fermi levels in the donor and acceptor domains and provide another mechanism for field-dependent charge generation yield. Finally, some fraction of the excited Frenkel excitons diffuse to the heterojunction interface, where they undergo charge separation.

Charge Separation: CT Exciton or CT Resonance. Importantly, the dynamics observed in either BHJ does not show strong evidence of the geminate recombination expected for CT excitons. This is true for PCDTBT:PC$_{70}$BM, where recombination dynamics is not pronounced, and in p-DTS(PTTh$_2$)$_2$:PC$_{70}$BM, where the recombination dynamics is

attributable to another cause. Two possible explanations are as follows: first, geminate recombination of the CT exciton may occur outside the window of our observations, and second, geminate recombination of the CT exciton may not occur in these systems. We prefer the latter explanation, noting that the internal quantum efficiency of PCDTBT:PC$_{70}$BM solar cells approaches 100%.[18]

Geminate recombination of CT excitons is observed and undoubtedly plays an important role in some material combinations, contributing to a loss of overall efficiency.[56−59] The important question is, how general is geminate recombination in organic heterojunctions? In some cases,[13,14,60] it appears that geminate recombination is not an important loss mechanism, forcing one to answer the question negatively. This is an observation that warrants comment, as simply considering the Coulomb binding of holes and electrons suggests that strongly bound pairs should be practically universal. It was recently shown that delocalization provides a rationale for low CT exciton binding energy and provides a means of efficient carrier generation.[14]

To further the discussion, we describe two possible scenarios of the CT exciton in Figure 10. Briefly, the diagrams in Figure
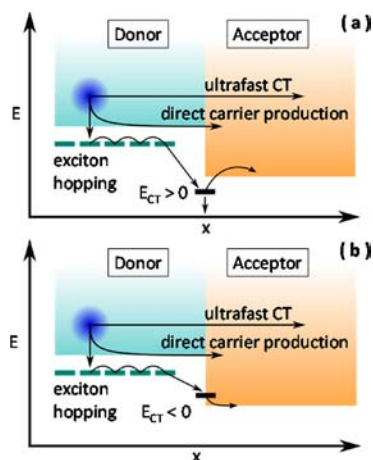
Figure 10. Schematic illustrations relevant to charge transfer processes. (a) Band diagram of the LUMO region of a heterojunction interface, where the CT exciton is a bound state. Lines indicate three methods of charge generation outlined above. (b) Identical to part a except that the CT exciton is not a bound state, but a resonance is comprised of mobile electrons in the acceptor domain and mobile holes into the donor domain.

10a,b represent the electronic states in the LUMO region of the energetic landscape. The binding energy of the CT exciton relative to electronic states in the acceptor (E_{CT}) is marked by a dash at the interface. Similar considerations apply to the hole. We note that Figure 10 is a schematic; quantitative arguments require a two-particle diagram.

In Figure 10a we consider the situation when the energy of the CT exciton is below the lowest energy states in the acceptor domain. Such a bound state can decay to the ground state by radiative emission, as has been reported in the literature.[56−59] In Figure 10b, we consider the situation when the energy of the CT exciton is greater than the lowest energy states in the acceptor domain. In this case, the CT exciton is not a bound state, but rather, it is a resonance that is comprised of mobile electrons in the acceptor domain and mobile holes into the

donor domain. We believe this situation to be operating to large measure in PCDTBT:PC$_{70}$BM.

More generally, bound CT exciton states will provide a mechanism for bimolecular decay in addition to geminate recombination as a result of the principle of microscopic reversibility. Thus, the CT state may also be important in understanding bimolecular decay, a dominant recombination process in many high-performing BHJ systems studied to date.[60−63] If one could control the width of the interface or increase the local dielectric constant so as to reduce the energy of the bound CT exciton and form the resonance state instead, the bimolecular recombination rate should be significantly reduced, deviating from Langevin recombination and increasing the fill factor of the BHJ solar cell. To understand the nature of the CT exciton in detail (bound state or resonance state), one needs a solution of the exciton problem in the presence of the asymmetric potential caused by the offset in the HOMO and LUMO energies of the donor and acceptor phases, a problem of significant difficulty.

■ CONCLUSION

In conclusion, the transient absorption dynamics of *p*-DTS(PTTh$_2$)$_2$:PC$_{70}$BM and PCDTBT:PC$_{70}$BM was studied. Both materials were found to be qualitatively similar in many respects. For example, both materials exhibit ultrafast carrier generation, which accounts for ∼70% of all photogenerated mobile carriers. This ultrafast charge transfer implies that the initial photoexcited wave functions are delocalized over distances comparable with the phase-separated domain size (>10−20 nm), as required by position−momentum uncertainty. In other words, the initial photoexcitation is delocalized but must undergo rapid localization, or wave function collapse, on the order of the decoherence time scale. If there is wave function amplitude at or near an interface, charge transfer can occur. This process is an important part of the carrier generation process in *p*-DTS(PTTh$_2$)$_2$:PC$_{70}$BM (and all BHJ systems studied), providing an explanation of the majority of the most rapidly generated carriers. The remaining ∼30% of photogenerated carriers were created by exciton diffusion to a charge-separating interface at times within 1−500 ps. Strong geminate recombination through bound CT exciton states was not observed on time scales less than 1.5 ns. To explain this observation, we noted the possibility that the CT exciton may not be a true bound state in every circumstance, but a resonance state comprised of mobile electrons and holes in their respective domains.

■ AUTHOR INFORMATION

Corresponding Author
lkaake@physics.ucsb.edu

Notes
The authors declare no competing financial interest.

■ REFERENCES

(1) He, Z.; Zhong, C.; Huang, X.; Wong, W.-Y.; Wu, H.; Chen, L.; Su, S.; Cao, Y. *Adv. Mater.* **2011**, *23*, 4636.

(2) Dou, L.; You, J.; Yang, J.; Chen, C.-C.; He, Y.; Murase, S.; Moriarty, T.; Emery, K.; Li, G.; Yang, Y. *Nat. Photonics* **2012**, *6*, 180.

(3) Small, C. E.; Chen, S.; Subbiah, J.; Amb, C. M.; Tsang, S.-W.; Lai, T.-H.; Reynolds, J. R.; So, F. *Nat. Photonics* **2012**, *6*, 115.

(4) van der Poll, T. S.; Love, J. A.; Nguyen, T.-Q.; Bazan, G. C. *Adv. Mater.* **2012**, *24*, 3646.

(5) Service, R. F. *Science* **2011**, *332*, 293.

(6) Bredas, J. L.; Norton, J. E.; Cornil, J.; Coropceanu, V. *Acc. Chem. Res.* **2009**, *42*, 1691.

(7) Clarke, T. M.; Durrant, J. R. *Chem. Rev.* **2010**, *110*, 6736.

(8) Howard, I. A.; Laquai, F. *Macromol. Chem. Phys.* **2010**, *211*, 2063.

(9) Roncali, J. *Acc. Chem. Res.* **2009**, *42*, 1719.

(10) Li, Y. W.; Guo, Q.; Li, Z. F.; Pei, J. N.; Tian, W. J. *Energy Environ. Sci.* **2010**, *3*, 1427.

(11) Welch, G. C.; Perez, L. A.; Hoven, C. V.; Zhang, Y.; Dang, X. D.; Sharenko, A.; Toney, M. F.; Kramer, E. J.; Nguyen, T. Q.; Bazan, G. C. *J. Mater. Chem.* **2011**, *21*, 12700.

(12) Sun, Y.; Welch, G. C.; Leong, W. L.; Takacs, C. J.; Bazan, G. C.; Heeger, A. J. *Nat. Mater.* **2012**, *11*, 44.

(13) Lee, J.; Vandewal, K.; Yost, S. R.; Bahlke, M. E.; Goris, L.; Baldo, M. A.; Manca, J. V.; Van Voorhis, T. *J. Am. Chem. Soc.* **2010**, *132*, 11878.

(14) Bakulin, A. A.; Rao, A.; Pavelyev, V. G.; van Loosdrecht, P. H. M.; Pshenichnikov, M. S.; Niedzialek, D.; Cornil, J.; Beljonne, D.; Friend, R. H. *Science* **2012**, *335*, 1340.

(15) Muntwiler, M.; Yang, Q.; Tisdale, W. A.; Zhu, X. Y. *Phys. Rev. Lett.* **2008**, *101*, 196403.

(16) Pensack, R. D.; Asbury, J. B. *J. Phys. Chem. Lett.* **2010**, *1*, 2255.

(17) Etzold, F.; Howard, I. A.; Mauer, R.; Meister, M.; Kim, T.-D.; Lee, K.-S.; Baek, N. S.; Laquai, F. *J. Am. Chem. Soc.* **2011**, *133*, 9469.

(18) Park, S. H.; Roy, A.; Beaupre, S.; Cho, S.; Coates, N.; Moon, J. S.; Moses, D.; Leclerc, M.; Lee, K.; Heeger, A. J. *Nat. Photonics* **2009**, *3*, 297.

(19) Wang, G. P.; Zhang, L.; Zhang, J. J. *Chem. Soc. Rev.* **2012**, *41*, 797.

(20) Braun, C. L. *J. Chem. Phys.* **1984**, *80*, 4157.

(21) Sun, Y. M.; Welch, G. C.; Leong, W. L.; Takacs, C. J.; Bazan, G. C.; Heeger, A. J. *Nat. Mater.* **2012**, *11*, 44.

(22) Kaake, L. G.; Welch, G. C.; Moses, D.; Bazan, G. C.; Heeger, A. J. *J. Phys. Chem. Lett.* **2012**, *3*, 1253.

(23) Tong, M. H.; Coates, N. E.; Moses, D.; Heeger, A. J.; Beaupre, S.; Leclerc, M. *Phys. Rev. B* **2010**, *81*, 125210.

(24) Albert-Seifried, S.; Friend, R. H. *Appl. Phys. Lett.* **2011**, *98*, 223304.

(25) Miranda, P. B.; Moses, D.; Heeger, A. J. *Phys. Rev. B* **2001**, *64*, 081201.

(26) Su, W. P.; Schrieffer, J. R. *Proc. Natl. Acad. Sci. U. S. A.-Phys. Sci.* **1980**, *77*, 5626.

(27) Kepler, R. G.; Valencia, V. S.; Jacobs, S. J.; McNamara, J. J. *Synth. Met.* **1996**, *78*, 227.

(28) Howard, I. A.; Hodgkiss, J. M.; Zhang, X.; Kirov, K. R.; Bronstein, H. A.; Williams, C. K.; Friend, R. H.; Westenhoff, S.; Greenham, N. C. *J. Am. Chem. Soc.* **2010**, *132*, 328.

(29) Hodgkiss, J. M.; Albert-Seifried, S.; Rao, A.; Barker, A. J.; Campbell, A. R.; Marsh, R. A.; Friend, R. H. *Adv. Funct. Mater.* **2012**, *22*, 1567.

(30) Sariciftci, N. S.; Smilowitz, L.; Heeger, A. J.; Wudl, F. *Science* **1992**, *258*, 1474.

(31) Brabec, C. J.; Zerza, G.; Cerullo, G.; De Silvestri, S.; Luzzati, S.; Hummelen, J. C.; Sariciftci, S. *Chem. Phys. Lett.* **2001**, *340*, 232.

(32) Grancini, G.; Polli, D.; Fazzi, D.; Cabanilas-Gonzalez, J.; Cerullo, G.; Lanzani, G. *J. Phys. Chem. Lett.* **2011**, *2*, 1099.

(33) Guo, J. M.; Ohkita, H.; Benten, H.; Ito, S. *J. Am. Chem. Soc.* **2010**, *132*, 6154.

(34) Etzold, F.; Howard, I. A.; Forler, N.; Cho, D. M.; Meister, M.; Mangold, H.; Shu, J.; Hansen, M. R.; Muellen, K.; Laquai, F. *J. Am. Chem. Soc.* **2012**, *134*, 10569.

(35) Mayer, A. C.; Toney, M. F.; Scully, S. R.; Rivnay, J.; Brabec, C. J.; Scharber, M.; Koppe, M.; Heeney, M.; McCulloch, I.; McGehee, M. D. *Adv. Funct. Mater.* **2009**, *19*, 1173.

(36) Collins, B. A.; Gann, E.; Guignard, L.; He, X.; McNeill, C. R.; Ade, H. *J. Phys. Chem. Lett.* **2010**, *1*, 3160.

(37) Miller, N. C.; Gysel, R.; Miller, C. E.; Verploegen, E.; Beiley, Z.; Heeney, M.; McCulloch, I.; Bao, Z. N.; Toney, M. F.; McGehee, M. D. *J. Polym. Sci., Part B* **2011**, *49*, 499.

(38) Treat, N. D.; Brady, M. A.; Smith, G.; Toney, M. F.; Kramer, E. J.; Hawker, C. J.; Chabinyc, M. L. *Adv. Energy Mater.* **2011**, *1*, 82.

(39) Liu, F.; Gu, Y.; Jung, J. W.; Jo, W. H.; Russell, T. P. *J. Polym. Sci., Part B* **2012**, *50*, 1018.

(40) Howard, I. A.; Mauer, R.; Meister, M.; Laquai, F. *J. Am. Chem. Soc.* **2010**, *132*, 14866.

(41) Smith, M. B.; Michl, J. *Chem. Rev.* **2010**, *110*, 6891.

(42) Rao, A.; Wilson, M. W. B.; Hodgkiss, J. M.; Albert-Seifried, S.; Bassler, H.; Friend, R. H. *J. Am. Chem. Soc.* **2010**, *132*, 12698.

(43) Chan, W.-L.; Ligges, M.; Jailaubekov, A.; Kaake, L.; Miaja-Avila, L.; Zhu, X.-Y. *Science* **2011**, *334*, 1541.

(44) Burdett, J. J.; Bardeen, C. J. *J. Am. Chem. Soc.* **2012**, *134*, 8597.

(45) Roberts, S. T.; McAnally, R. E.; Mastron, J. N.; Webber, D. H.; Whited, M. T.; Brutchey, R. L.; Thompson, M. E.; Bradforth, S. E. *J. Am. Chem. Soc.* **2012**, *134*, 6388.

(46) Yang, X. J.; Dykstra, T. E.; Scholes, G. D. *Phys. Rev. B* **2005**, *71*, 045203.

(47) Hwang, I.; Scholes, G. D. *Chem. Mater.* **2011**, *23*, 610.

(48) Fluegel, B.; Peyghambarian, N.; Olbright, G.; Lindberg, M.; Koch, S. W.; Joffre, M.; Hulin, D.; Migus, A.; Antonetti, A. *Phys. Rev. Lett.* **1987**, *59*, 2588.

(49) Jasieniak, J. J.; Hsu, B. B. Y.; Takacs, C. J.; Welch, G. C.; Bazan, G. C.; Moses, D.; Heeger, A. J. *ACS Nano* **2012**, *6*, 8735.

(50) Kaake, L. G.; Barbara, P. F.; Zhu, X. Y. *J. Phys. Chem. Lett.* **2010**, *1*, 628.

(51) Heeger, A. J.; Kivelson, S.; Schrieffer, J. R.; Su, W. P. *Rev. Mod. Phys.* **1988**, *60*, 781.

(52) Tao, S.; Matsuzaki, H.; Uemura, H.; Yada, H.; Uemura, T.; Takeya, J.; Hasegawa, T.; Okamoto, H. *Phys. Rev. B* **2011**, *83*, 075204.

(53) Arias, A. C.; MacKenzie, J. D.; McCulloch, I.; Rivnay, J.; Salleo, A. *Chem. Rev.* **2010**, *110*, 3.

(54) Yamagata, H.; Norton, J.; Hontz, E.; Olivier, Y.; Beljonne, D.; Bredas, J. L.; Silbey, R. J.; Spano, F. C. *J. Chem. Phys.* **2011**, *134*, 204703.

(55) Lakowicz, J. R. *Principles of Fluorescence Spectroscopy*; Springer: New York, 2006.

(56) Loi, M. A.; Toffanin, S.; Muccini, M.; Forster, M.; Scherf, U.; Scharber, M. *Adv. Funct. Mater.* **2007**, *17*, 2111.

(57) Morteani, A. C.; Sreearunothai, P.; Herz, L. M.; Friend, R. H.; Silva, C. *Phys. Rev. Lett.* **2004**, *92*, 247402.

(58) Huang, Y. S.; Westenhoff, S.; Avilov, I.; Sreearunothai, P.; Hodgkiss, J. M.; Deleener, C.; Friend, R. H.; Beljonne, D. *Nat. Mater.* **2008**, *7*, 483.

(59) Tvingstedt, K.; Vandewal, K.; Zhang, F. L.; Inganas, O. *J. Phys. Chem. C* **2010**, *114*, 21824.

(60) Kniepert, J.; Schubert, M.; Blakesley, J. C.; Neher, D. *J. Phys. Chem. Lett.* **2011**, *2*, 700.

(61) Cowan, S. R.; Roy, A.; Heeger, A. J. *Phys. Rev. B* **2010**, *82*, 245207.

(62) Street, R. A.; Cowan, S.; Heeger, A. J. *Phys. Rev. B* **2010**, *82*, 121301.

(63) Albrecht, S.; Schindler, W.; Kurpiers, J.; Kniepert, J.; Blakesley, J. C.; Dumsch, I.; Allard, S.; Fostiropoulos, K.; Scherf, U.; Neher, D. *J. Phys. Chem. Lett.* **2012**, *3*, 640.